



Some Lewis acid-base adducts involving boron trifluoride as electrolyte additives for lithium ion cells

Mengyun Nie, L. Madec, J. Xia, D.S. Hall, J.R. Dahn*

Dept. of Physics and Atmospheric Science, Dalhousie University, Halifax, B3H4R2 Nova Scotia, Canada



HIGHLIGHTS

- Describes several Lewis acid-base adducts as electrolyte additives.
- Pyridine boron trifluoride is the best adduct studied here.
- Pyridine boron trifluoride improved storage, impedance and long-term cycling.

ARTICLE INFO

Article history:

Received 27 April 2016

Received in revised form

23 July 2016

Accepted 9 August 2016

Available online 17 August 2016

Keywords:

Lithium ion cells

Electrolyte additives

Lewis acid-base complexes

NMC/graphite pouch cells

ABSTRACT

Three complexes with boron trifluoride (BF_3) as the Lewis acid and different Lewis bases were synthesized and used as electrolyte additives in $\text{Li}[\text{Ni}_{1/3}\text{Mn}_{1/3}\text{Co}_{1/3}]O_2/\text{graphite}$ and $\text{Li}[\text{Ni}_{0.42}\text{Mn}_{0.42}\text{Co}_{0.16}]O_2/\text{graphite}$ pouch cells. Lewis acid-base adducts with a boron-oxygen (B–O) bond were trimethyl phosphate boron trifluoride (TMP-BF) and triphenyl phosphine oxide boron trifluoride (TPPO-BF). These were compared to pyridine boron trifluoride (PBF) which has a boron-nitrogen (B–N) bond. The experimental results showed that cells with PBF had the least voltage drop during storage at 4.2 V, 4.4 V and 4.7 V at 40 °C and the best capacity retention during long-term cycling at 55 °C compared to cells with the other additives. Charge-hold-discharge cycling combined with simultaneous electrochemical impedance spectroscopy measurements showed that impedance growth in TMP-BF and TPPO-BF containing cells was faster than cells containing 2%PBF, suggesting that PBF is useful for impedance control at high voltages (>4.4 V). XPS analysis of the SEI films highlighted a specific reactivity of the PBF-derived SEI species that apparently hinders the degradation of both LiPF_6 and solvent during formation and charge-hold-discharge cycling. The modified SEI films may explain the improved impedance, the smaller voltage drop during storage and the improved capacity retention during cycling of cells containing the PBF additive.

© 2016 Elsevier B.V. All rights reserved.

1. Introduction

Incorporating electrolyte additives into the electrolyte of Li-ion batteries (LIBs) is one effective method for extending their lifetime [1–3]. Pyridine boron trifluoride (PBF) and other aromatic amine:boron trifluoride complexes have been proposed and tested as electrolyte additives for NMC-based LIBs [4–8]. Several of these additives have been demonstrated to improve LIB performance during cycling and storage at high temperatures. Recently, possible chemical pathways for solid-electrolyte interphase (SEI) formation on the negative electrode surface in PBF-containing cells were

investigated using density functional theory (DFT) and a variety of experimental techniques [9]. However, the actual mechanisms by which the BF_3 and/or the aromatic amine groups in PBF-type additives improve cell performance are not yet understood. Thus far, untested hypotheses about the roles of the different functional groups are based on statements found in Refs. [10–13]. BF_3 , as a boron-based anion receptor, might react with insoluble LiF from the SEI layers on the positive and/or negative electrodes to form the soluble electrolyte salt LiBF_4 [10,11]. This would rationalize the observation that PBF limits impedance growth during cycling [6,7]. Aromatic amines are widely used as corrosion inhibitors for metals including iron, steel and copper in acidic environments [12,13], so those Lewis base amines might help prevent transition metal dissolution from NMC positive electrodes by neutralizing acidic impurities in the electrolyte. All the aromatic amine: BF_3 Lewis

* Corresponding author.

E-mail address: jeff.dahn@dal.ca (J.R. Dahn).

adducts were synthesized by mixing the amine with $\text{BF}_3\text{Et}_2\text{O}$ to obtain solid products with a boron-nitrogen bond [14,15].

Moreover, electrolyte additives are not limited to aromatic amine: BF_3 adducts. Researchers at E-one Moli Energy Canada [16] and at Toyota [17] patented carbonate: BF_3 adducts that contain one boron atom bonded to one oxygen atom. Matsui et al. [17] studied asymmetric BF_3 adducts, which can be used as electrolyte solvents due to their wide potential window and excellent oxidation resistance. In this work, trimethyl phosphate boron trifluoride (TMP-BF) and triphenyl phosphine oxide boron trifluoride (TPPO-BF), each of which has a boron-oxygen bond, were synthesized. These were tested as electrolyte additives in $\text{Li}[\text{Ni}_{1/3}\text{Mn}_{1/3}\text{Co}_{1/3}]\text{O}_2/\text{graphite}$ and $\text{Li}[\text{Ni}_{0.42}\text{Mn}_{0.42}\text{Co}_{0.16}]\text{O}_2/\text{graphite}$ pouch cells and compared to PBF. The motivation of this work is to test the effect of retaining the Lewis acid (BF_3) from PBF and modifying the nature of the Lewis base (pyridine). This work is complementary to recent studies that utilized pyridine phosphorus pentafluoride (PPF), in which the Lewis base (pyridine) was retained and it was the Lewis acid (PF_5) that was modified [8,9]. The behavior of PBF- and PPF-containing cells are generally similar, although some differences have been noted. It is heretofore unknown whether this indicates that it is the pyridine species that is responsible for the performance of PBF-containing cells, or whether the two Lewis acids (BF_3 and PF_5) are simply so chemically similar that they may play the same role in a Li-ion cell.

2. Experimental

2.1. Synthesis of the Lewis acid-base adducts

The synthesis procedure for the Lewis acid-base adducts is shown in **Scheme 1**.

Trimethyl phosphate boron trifluoride (TMP-BF): To a 50 ml round bottom flask, 2.5 g of boron trifluoride etherate ($\text{BF}_3\text{Et}_2\text{O}$, > 46.5% BF_3 , Sigma-Aldrich) was dissolved in 10.0 mL hexane, then 2.0 g of trimethyl phosphate (Sigma-Aldrich, > 99%) was added to the solution dropwise, and transparent crystals of the TMP-BF complex formed gradually at the bottom of the flask and were collected by removing the solvent. The solid samples were further

rinsed with hexane and dried in vacuum (40°C) overnight.

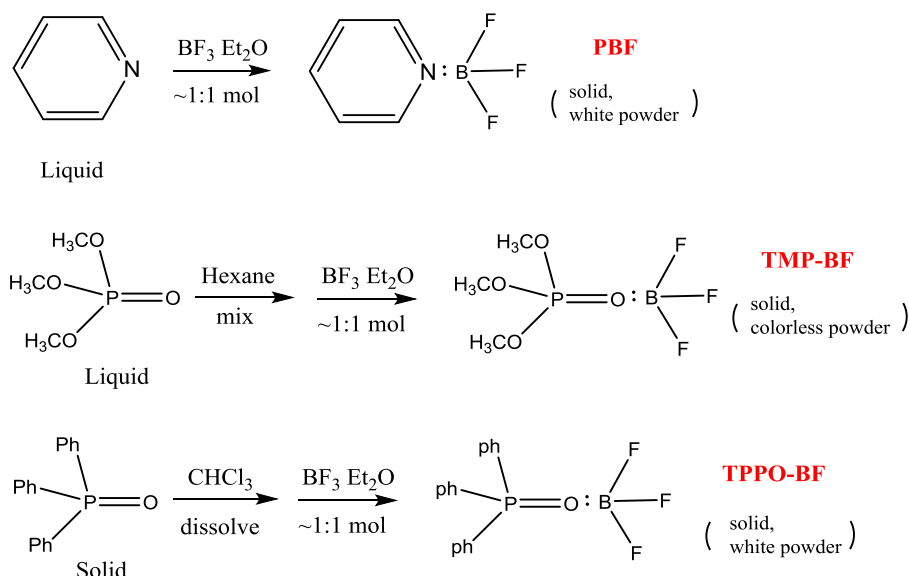
Triphenyl phosphine oxide boron trifluoride (TPPO-BF): The synthesis of TPPO-BF was similar to the synthesis of pyrazine diboron trifluoride reported earlier [5,6]. **1.0** g (0.0036 mol) triphenyl phosphine oxide (Sigma-Aldrich, >98%) in **2** mL chloroform was added slowly into 1.0 mL $\text{BF}_3\text{Et}_2\text{O}$. The reaction was highly exothermic so the reaction bottle was kept near room temperature by the slow addition of the reagents. White or colorless crystals normally precipitated out immediately, but if no precipitate was observed then the reaction mixture was transferred to a -20°C freezer and crystals then formed. The solid products were then rinsed by chloroform twice and collected by filtration. The wet product was transferred to a vacuum oven and vacuum dried overnight at $45-50^\circ\text{C}$.

Pyridine boron trifluoride (PBF) was synthesized as previously described [4]. **Table 1** lists the affinity constants of several Lewis acid-base adducts involving BF_3 [14]. The affinity constants are an indicator of the Lewis acid-base bond strength. Larger affinity constants correspond to stronger bonds. In this work, Lewis acid-base adducts showing higher affinity constants than $\text{BF}_3\text{Et}_2\text{O}$ were targeted so that the exchange with Et_2O is spontaneous. The purity of the synthesized TMP-BF and TPPO-BF after vacuum drying was checked by NMR (^1H , ^{19}F , ^{11}B) and no peaks of the initial reactants were observed in the NMR spectra in **Figs. S1 and S2**. The NMR spectra of PBF can be found in the supporting information of reference 4.

Table 1
Affinity constants of various Lewis acid-base Complexes.

Lewis base	Abbre.	BF_3 affinity (kJ mol^{-1})
Pyridine	Pyr	128.08 ± 0.50^{14}
Diethyl ether	Et_2O	78.77 ± 0.36^{14}
Trimethyl phosphate	TMP	84.75 ± 0.22^{14}
Triphenyl phosphine oxide	TPPO	103.30 ± 1.50^{14}
Ethylene carbonate	EC	66.40 ± 1.10^{14}

BF_3 affinities (kJ mol^{-1}) of Lewis bases in dichloromethane at 298 K and 1 atm .



Scheme 1. Synthesis procedure and structure of pyridine boron trifluoride (PBF), trimethyl phosphate boron trifluoride (TMP-BF), and triphenyl phosphine oxide boron trifluoride (TPPO-BF).

2.2. Pouch cells and electrolyte preparation

1 M LiPF₆ in ethylene carbonate/ethyl methyl carbonate (EC/EMC, 3:7 wt% ratio, BASF) was used as the control electrolyte in the studies reported here. To this electrolyte, the Lewis acid-base adducts, listed in Table 2, were added. Additive components were added at specified weight percentages in the electrolyte. Other standard electrolyte additives were also used for comparison. These included vinylene carbonate (VC, BASF, 99.97%) and prop-1-ene,1,3-sultone (PES, Lianchuang Medicinal ChemistryCo., 98.20%).

Dry Li[Ni_{1/3}Mn_{1/3}Co_{1/3}]O₂ (NMC111)/graphite pouch cells (220 mAh) balanced for 4.4 V and LaPO₄-coated and uncoated Li[Ni_{0.42}Mn_{0.42}Co_{0.16}]O₂ (NMC442)/graphite pouch cells (180 mAh/240 mAh) balanced for 4.7 V operation were obtained without electrolyte from Li-Fun Technology (Xinma Industry Zone, Golden Dragon Road, Tianyuan District, Zhuzhou City, Hunan Province, PRC, 412000, China). The LaPO₄-coated Li[Ni_{0.42}Mn_{0.42}Co_{0.16}]O₂ was prepared at 3 M Co. by coating 3 wt % LaPO₄ on Li[Ni_{0.42}Mn_{0.42}Co_{0.16}]O₂ provided by Umicore. The same Li[Ni_{0.42}Mn_{0.42}Co_{0.16}]O₂, without coating, was used in the uncoated NMC442/graphite cells. All pouch cells were vacuum sealed without electrolyte in China and then shipped to our laboratory in Canada. Before electrolyte filling, the cells were cut just below the heat seal and dried at 80 °C under vacuum for 14 h to remove any residual water. Then the cells were transferred immediately to an argon-filled glove box for filling and vacuum sealing. The NMC/graphite pouch cells were filled with 0.9 g of electrolyte. After filling, cells were vacuum-sealed with a compact vacuum sealer (MSK-115A, MTI Corp.). First, cells were placed in a temperature box at 40. ± 0.1 °C, where they were held at 1.5 V for 24 h, to allow for the completion of wetting. Then, cells were charged at 11 mA (C/20) to 3.5 V. After this step, cells were transferred and moved into the glove box, cut open to release gas generated and then vacuum sealed again. After degassing, impedance spectra of the cells were measured at 3.8 V as described below. The NMC442/graphite cells destined for 4.4 or 4.5 V operation were degassed a second time at 4.5 V. The amounts of gas created during formation to 3.5 V and between 3.5 V and 4.5 V were measured and recorded.

2.3. Electrochemical impedance spectroscopy

Electrochemical impedance spectroscopy (EIS) measurements were conducted on NMC/Graphite pouch cells before and after storage and also after long-term cycling. Cells were charged or discharged to 3.80 V before they were moved to a 10. ± 0.1 °C temperature box. AC impedance spectra were collected with ten points per decade from 100 kHz to 10 mHz with a signal amplitude of 10 mV at 10. ± 0.1 °C. A Biologic VMP-3 was used to collect this data.

2.4. Charge-hold-discharge cycling with simultaneous electrochemical impedance spectroscopy

Some cells were tested extremely aggressively to really push the limits of the electrolyte. Two different cycling protocols were used (1): The cells were charged and discharged at 44 mA between 2.8

and 4.4 V and held at 4.4 V for 20 h (2): The cells were charged and discharged at 100 mA between 2.8 and 4.5 V and held at 4.5 V for 24 h. Both protocols were carried out at 40 °C. Automated impedance spectroscopy measurements were made after every three charge-hold-discharge cycles using a frequency response analyzer (FRA)/cycler system built at Dalhousie University [18]. During FRA measurements, the cells were charged and discharged at 24 mA (C/10) and AC impedance spectra were collected every 0.1 V. In this paper, the (combined) diameter of the semicircle(s) in the Nyquist plot is called the charge transfer resistance, R_{ct}, and represents contributions from the transport of ions from the electrolyte through the SEI layer to combine with electrons in the active material at both electrodes.

2.5. Storage experiments

The cycling/storage procedure used in these tests is described as follows. Due to the different target storage potentials, different types of NMC/graphite cells were used for different storage experiments. NMC111/graphite pouch cells balanced at 4.4 V were used for 4.2 V storage and NMC442/graphite pouch cells balanced to 4.7 V were used for 4.4 V storage. LaPO₄-coated NMC442/graphite cells were used for 4.7 V storage [19,20]. Cells were first charged to 4.2, 4.4 or 4.7 V and discharged to 2.8 V two times. Then the cells were charged to 4.2, 4.4 or 4.7 V at a current of C/20 (11 mA) and then held at 4.2, 4.4 or 4.7 V for 24 h. A recent in-situ neutron diffraction study of NMC442 pouch cells held at 4.7 V shows that no structural degradation to the bulk NMC442 structure occurs during hold at 4.7 V [21]. A Maccor series 4000 cycler was used for the preparation of the cells prior to storage. After the pre-cycling process, cells were carefully moved to the storage system which monitored their open circuit voltage every 6 h for a total storage time of 500 h [22]. Storage experiments were made at 40. ± 0.1 °C.

2.6. Long-term cycling

Long term cycling was conducted with an upper cutoff potential of 4.4 V. The cells were continuously charged and discharged at 80 mA (C/3) between 2.8 and 4.4 V at 55. ± 0.1 °C using a Neware (Shenzhen, China) charger system.

2.7. Determination of volume of gas evolved in pouch cells

Ex-situ (static) gas measurements were made using Archimedes' principle and used to measure gas evolution during formation and during cycling as described in Ref [23].

3. X-ray photoelectron spectroscopy (XPS)

3.1. Sample preparation

After electrochemical test, pouch cells were carefully disassembled in an argon-filled glove box within 12 h following the end of the electrochemical process. Graphite and NMC442 electrodes were cut from the pouch cell electrodes with a precision

Table 2

Physical properties of Lewis acid-base complexes used in electrolytes.

Product (electrolyte additive)	Short name	Purity (based on NMR)	Solubility in EC:EMC (3:7)
Pyridine boron trifluoride	PBF	>99%	>2%
Trimethyl phosphate boron trifluoride	TMP-BF	>99%	>2%
Triphenyl phosphine oxide boron trifluoride	TPPO-BF	>98%	Aprox 1%

punch and rinsed twice by immersion into 0.8 mL of EMC solvent (BASF) in a clean and dry glass vial with a mild manual agitation for 10 s to remove the majority of the LiPF₆ salt. Air-sensitive samples were then mounted onto a molybdenum holder using a copper conductive tape (3 M Co.) under argon and placed into a special transfer system as described in Ref. [24]. The latter was then put under vacuum at approx. 10⁻³ mbar for 1 h and then connected to the spectrometer where samples were loaded under a pressure of ~10⁻³ mbar. All samples were kept at 10⁻⁸ mbar for one night before analysis to allow a strictly identical vacuum procedure.

3.2. Data acquisition and treatment

XPS was performed on a SPECS spectrometer equipped with a Phoibos 150 hemispherical energy analyzer and using Mg K α radiation ($h\nu = 1253.6$ eV). The analyzed sample area was $\sim 2 \times 3$ mm² which gives results representative of the whole electrode. Core spectra were recorded in the fixed analyzer transmission (FAT) mode with a 20 eV pass energy at an operating pressure $< 2 \times 10^{-9}$ mbar. Short acquisition time spectra were first recorded as references to follow any possible sample degradation during the analysis. Data treatment was performed using CasaXPS software. The binding energy scale was calibrated from the C1s peak at 285 eV (C—C/C—H) and the O1s peak at 529.6 eV (O²⁻ anion from the NMC) for the graphite and NMC electrodes respectively. A nonlinear Shirley-type background [25] was used for core peak analysis while 70% Gaussian – 30% Lorentzian Voigt peak shapes and full width at half-maximum (fwhm) constraint ranges were selected to optimized areas and peak positions.

4. Results and discussion

Fig. 1a shows the voltage of the NMC442/graphite cells with

different additives as indicated as the function of capacity during the first charge to the first degassing point (3.5 V). Fig. 1b shows the differential capacity versus voltage for the same cells. Fig. 1 compares the TMP-BF and TPPO-BF (B—O bond containing additives) and PBF (the B—N containing additive). Fig. 1a and b shows cells with 1% and 2% TMP-BF or TPPO-BF had the same voltage vs. capacity and dQ/dV vs. V curves as the control electrolyte (no additives), suggesting that those additives are not reduced before EC reduction. Fig. 1b shows the PBF-containing cells had a differential capacity (dQ/dV) peak at 2.3 V (negative electrode potential ≈ 1.2 V vs Li/Li⁺) and that the intensity of this peak increased with PBF content. Therefore, the 2.3 V peak is related to the reduction of PBF on the graphite surface, as reported previously [4,6,9]. Fig. 1b shows that for all electrolyte solution chemistries tested in this work, there is a peak at 2.9 V (≈ 0.8 V vs Li/Li⁺), corresponding to the reduction of EC on the graphite surface to form various lithium carbonate salts and ethene gas [26–28]. It is unknown what effect a PBF-derived SEI has, if any, on the electrochemical reduction of EC in a full cell. However, the results in Fig. 1b suggest that the presence of a PBF-derived SEI does not form a passivation layer that prevents solvent reduction, as is the case for many other sacrificial electrolyte additives (e.g., VC or PES) [29–32].

Fig. 1c shows the amount of gas evolved during formation of the cells described in Fig. 1a. All cells show a similar amount of gas which is suspected to be primarily ethene from EC reduction [27]. This supports the hypothesis that the PBF-derived SEI does not significantly prevent the EC reduction reaction which is normally accompanied by this gas production. In contrast, passivating additives such as VC and PES inhibit this gas evolution step [27]. Fig. 1d shows R_{ct} of all the cells after formation. The cells with 2% PBF have much larger impedance after formation than the cells with the other additives. This may be attributable to the formation of an additional SEI component from the reduction of PBF at the graphite

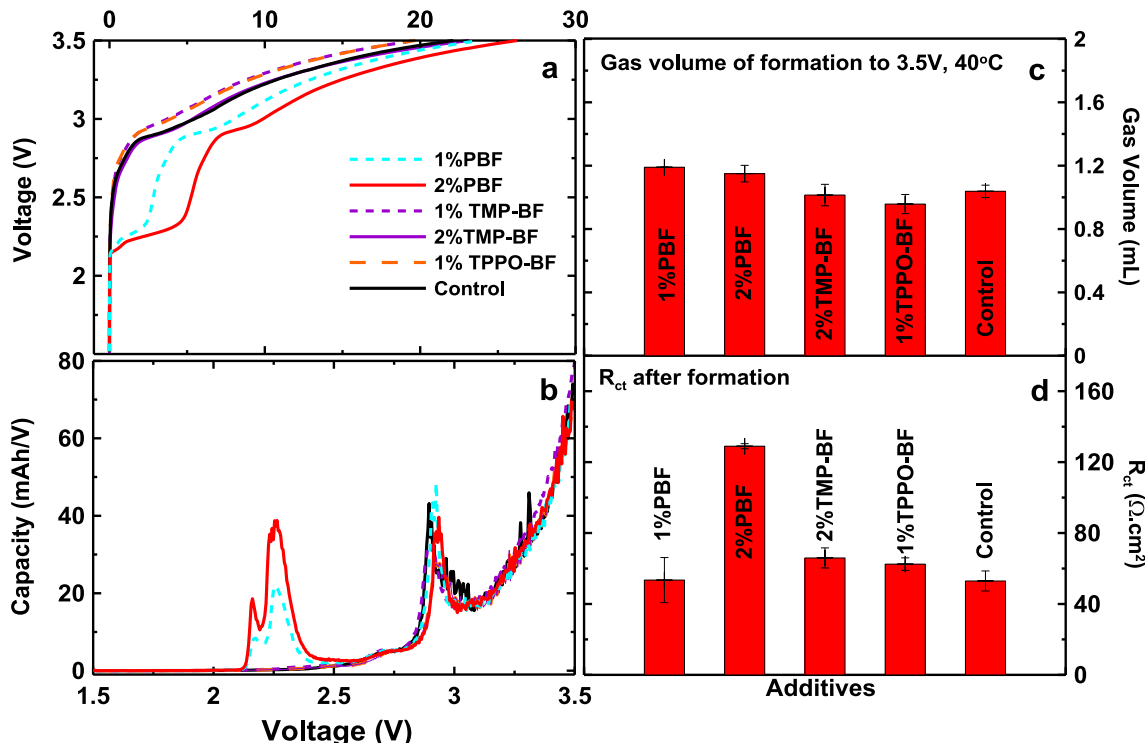


Fig. 1. (a) The cell voltage as a function of capacity during the initial charge (formation cycle) to the first degassing point (3.5 V); (b) differential capacity (dQ/dV) versus voltage (V) during the same formation process for NMC442/graphite pouch cells containing different additives; (c) gas evolution during formation to 3.5 V of pouch cells with selected electrolytes used in this work and (d) R_{ct} of the cells with different electrolytes after formation.

surface.

Fig. 2 shows the open circuit voltage (OCV) versus time during storage at 40 °C for NMC111/graphite pouch cells at 4.2 V, NMC442/graphite cells at 4.4 V and LaPO₄-coated NMC442/graphite pouch cells at 4.7 V. The LaPO₄-coated NMC442/graphite cells have been shown to operate better at high potential than uncoated NMC442/graphite cells if control electrolyte is used [19]. However, if modern electrolyte additives are used, the benefit of the coating is unclear [20]. Fig. 2a shows that at 4.2 V, NMC111/graphite cells with 2% PBF have the smallest voltage drop after 500 h compared to cells with TMP-BF, TPPO-BF, 2% VC or control electrolytes. The cells with 2% TMP-BF showed more voltage drop than 1% PBF and 2% VC cells. 1% TPPO-BF cells have a much larger voltage drop than the other

additives. Nonetheless, the voltage drop is significantly less than measured for the control cells. These results clearly demonstrate that the introduction of three chemically distinct BF₃ adduct additives improve the OCV storage behavior of cells. One interpretation of this observation is that the introduction of the Lewis acid species (BF₃) into a cell is responsible, at least in part, for an improvement to storage performance at 4.2 V. It remains undemonstrated how a Lewis acid such as BF₃ or PF₅ may lead to this improvement. Fig. 2b shows the impedance of the same NMC111/graphite cells after the 4.2 V storage period. The data indicate that the cells with 2% TMP-BF and 1% TPPO-BF have smaller impedance than 2% PBF and VC cells. Cells with 2% PBF had the largest impedance after 4.2 V storage.

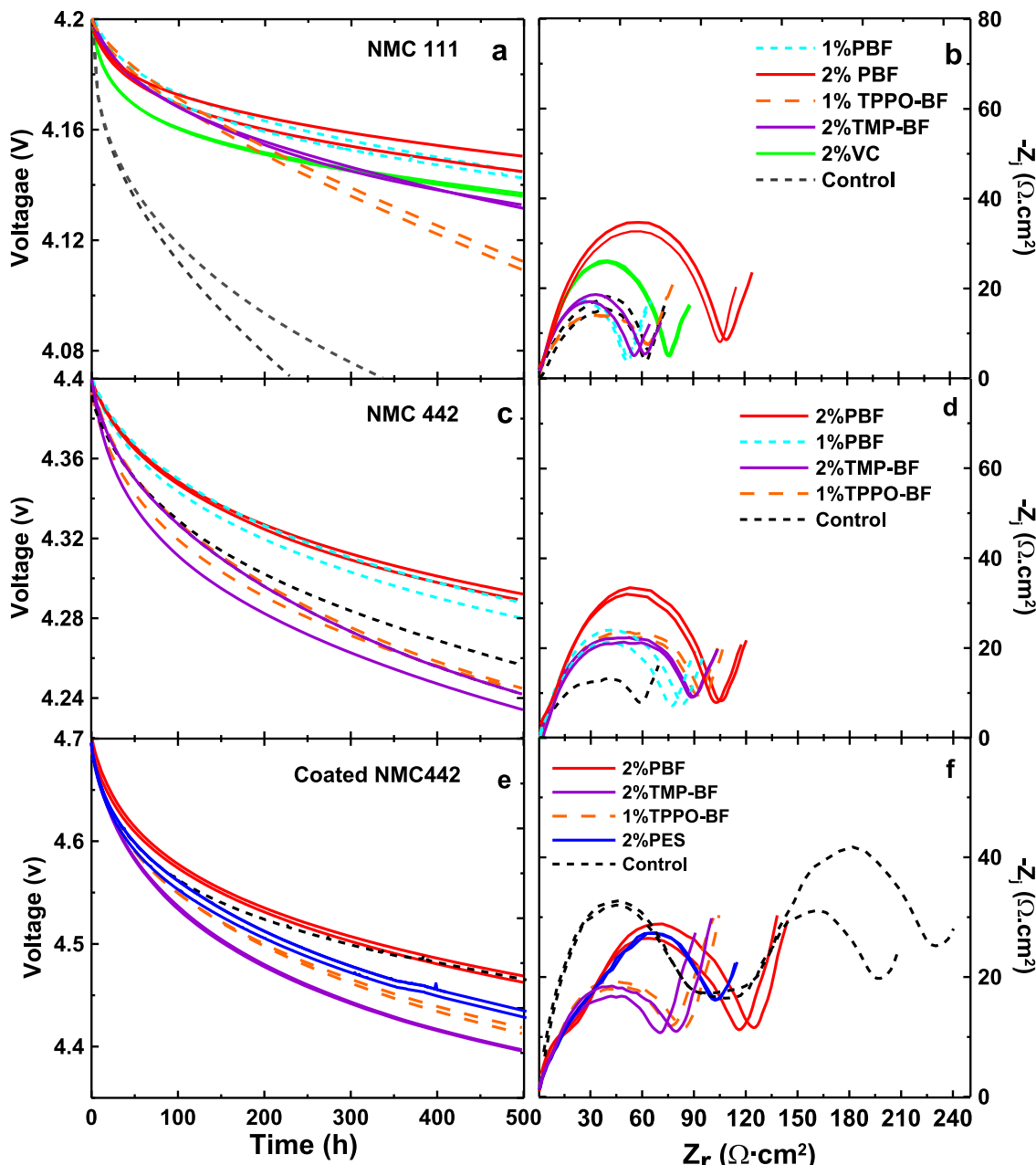


Fig. 2. (a) Open circuit voltage versus time of NMC111/graphite pouch cells stored at 4.2 V and 40 °C with different additives; (b) the corresponding impedance spectra of the same cells after 4.2 V storage; (c) OCV vs. time of NMC442/graphite pouch cells stored at 4.4 V and 40 °C with PBF, TMP-BF, TPPO-BF and control electrolytes; (d) the corresponding impedance spectra of the same cells after 4.4 V storage; (e) OCV vs. time of LaPO₄-coated NMC442/graphite pouch cells stored at 4.7 V with the selected electrolytes at 40 °C and (f) the corresponding impedance spectra of the same coated cells after 4.7 V storage.

In contrast to the previous results, Fig. 2c shows no consistent storage improvement at 4.4 V NMC442/graphite cells containing 2% PBF have the smallest voltage drop of the solution chemistries tested in this work, whereas cells with 2% TMP-BF or 1% TPPO-BF performed worse than cells filled with control electrolytes during 4.4 V storage. This result is significant, because it demonstrates that the Lewis acid alone, which was BF_3 for the three additives in this work, does not consistently lead to improved storage performance. Among all additives, cells containing 2% PBF have the largest impedance after storage while control cells have the smallest impedance.

Fig. 2e shows the storage results of the LaPO_4 -coated NMC442/graphite cells at 4.7 V. Cells with additives show similar or worse storage performance than that of control cells. The storage test at 4.7 V is very tough and the benefits of many additives in storage apparently disappear as has been seen in previous work from our group (for example see Fig. 2 in the paper by Ma et al. [33]) Fig. 2f shows the impedance of the cells after storage at 4.7 V. The impedance spectra of the control cells changed dramatically compared to 4.2 and 4.4 V storage, showing two distinguishable semicircles, while those of the cells containing PES or BF_3 -containing additives did not. The impedance spectra of TMP-BF and TPPO-BF cells are quite similar to their corresponding results in Fig. 2d, perhaps due to the large voltage drop causing the cells to stay at lower voltage most of storage time. Based on the results in Fig. 2e and f, 2% PBF yields best combination of high potential during storage at 4.7 V and impedance control.

Fig. 3 shows a summary of the FRA data of NMC442/graphite cells with different electrolytes tested to 4.5 V at 40 °C. Fig. 3a shows the discharge capacity versus cycle number of 2% PBF, 2% TMP-BF, 1% TPPO-BF and control cells undergoing an extremely aggressive charge-hold-discharge protocol as shown in Fig. 3b. The cells were clamped to limit the impact of any possible gas evolution on cycling performance. The capacity of the control cell fades very quickly and it lost 100% of its capacity after 50 cycles, which resulted from a dramatic increase of R_{ct} during cycling as shown previously [4,5]. Cells containing 1% TPPO-BF or 2% TMP-BF are generally similar during the first 30 cycles and then the capacity fade rate of TMP-BF accelerates after 40 cycles. However, they show much better capacity retention than control cells. This may indicate that the introduction of the Lewis acid BF_3 is beneficial, but it also clearly demonstrates that the nature of the Lewis base can significantly affect cycling performance. Cells containing 2% PBF showed the best capacity retention and cells containing 2% PBF lost less than 20% capacity fade during the 50 cycles (over 2 months).

Fig. 3c–k shows the raw impedance spectra as measured by the FRA. Fig. 3c shows the impedance spectra of 2% PBF cells measured at 4.4 V every 6 cycles; Fig. 3d shows the impedance spectra for the same cell measured at 3.8 V and Fig. 3e shows a summary of impedance spectra measured at various potentials during the last cycle (cycle 50). Similarly, Fig. 3f, g and h show some of the raw impedance spectra of the cell containing 1% TPPO and Fig. 3i, j and k show the some of the spectra of the cell containing 2% TMP. All the spectra have inductive tails at high frequency due to the internal inductance of the measurement device used to collect the data [34]. The solid blue spectrum represents the impedance measured during the first cycle of the cells and the solid and dashed red spectra were measured during the last cycle at 3.8 and 4.4 V, respectively. From blue to red, the shift of high frequency spectra to the right indicates an increase of electrolyte or electronic resistance.

All the spectra in Fig. 3c–k distorted to two “semicircles” at both 3.8 and 4.4 V as the cycle number increased but the distortion was more dramatic at higher potential. Fig. 3c, f and i show that huge low frequency semicircles developed at low frequencies which are associated with the growth of the positive electrode SEI. Fig. 3e, h

and k demonstrate the dynamic nature of the positive electrode SEI with potential as the low frequency semicircle is dramatically reduced in size as the potential decreases from 4.5 V to 3.8 V Fig. 3d, g and j show that the impedance at 3.8 V increased in cells with 2% PBF to cells with 1% TPPO-BF to and finally to cells with 2% TMP-BF. It is our opinion that this impedance increase, which is exactly in the same order as the capacity loss in Fig. 3a is responsible for the poor capacity retention of the TPPO-BF and TMP-BF containing cells compared to the PBF containing cells.

Fig. 3d, g and j also show that the high frequency “semicircle” increases in diameter and size as cycling proceeds. Fig. 3e, h and k show that the size of the high frequency semicircle does not change with potential during the same cycle. The high frequency semicircle is normally attributed to the contact resistance of the positive electrode to the current collectors [35–37] and the slow increase during this aggressive cycling suggests this contact needs to be improved in future work. Readers who are concerned about the assignment of the two semicircles in each of Fig. 3c–k are invited to read the work of Petibon et al. [38], where symmetric cells were used to show that impedance growth in NMC/graphite cells at high voltage (>4.4 V) is dominated by the positive electrode.

Fig. 4a shows analogous data to Fig. 3a, except cells were tested to an upper limit of 4.4 V as shown by the protocol in Fig. 4b. As in Fig. 3, control cells perform very poorly and cells with 2% PBF perform very well. After the charge-hold-discharge cycling shown in Fig. 4, the cells containing additives were then charged and discharged twice at C/50. This was done to investigate the source of capacity fade shown in Fig. 4a. The capacity of the cells during the C/50 cycles recovered to ~200, ~220 and ~240 mAh for the 2% TMP-BF, 1% TPPO-BF and 2% PBF-containing cells, respectively. This suggests that impedance growth is the major reason for the capacity fade during the charge-hold-discharge cycling and not loss of lithium inventory. Unfortunately similar low rate experiments were not performed for them.

Fig. 5a, b and c summarize the gas evolved in the cells after 4.2, 4.4 and 4.7 V storage. During storage at 4.2 or 4.4 V, the cells have no swelling problem since the amount of evolved gas is less than 0.1 mL which is less than 5% of the total cell volume (2.2 mL). During 4.7 V storage, all the cells with additives evolved more than 0.2 mL gas and cells with additives generated even more gas than control cells. The quantity of gas evolved is similar for cells prepared with each of the three adduct compounds or with PES, but is about twice that measured for control cells. Fig. 5e and d shows the amount of gas evolved from the cells during the charge-hold-discharge cycling described by Figs. 3 and 4. Cells containing 2% TMP-BF and 1% TPPO-BF produced more than 0.4 mL gas while cells containing 2% PBF and control electrolyte produced ~0.2 mL during charge-hold-discharge cycling at 4.4 V. However, when the cutoff voltage was increased to 4.5 V significantly more gas was produced by the control (~1.3 mL), 2% TMP (~1.0 mL) and 1% TPPO (0.9 mL) cells compared to the 2% PBF cell (~0.3 mL). These results reaffirm the conclusion that the role of these additives depend on the nature of the Lewis base. However, it is proposed that it is the ability of the base to form an SEI layer that is important, rather than its basicity.

Fig. 6a and b shows the discharge capacity and charge-discharge polarization, ΔV , vs cycle number for uncoated NMC442/Graphite cells during long-term cycling between 2.8 V and 4.4 V at 55.0 °C using currents corresponding to C/3 (80 mA). Control cells and cells with 2% TMP-BF show rapid capacity fade and impedance growth during the test. Just as in the charge-hold-discharge experiments described by Fig. 4, the cell containing 2% PBF shows the best capacity retention and the smallest increase in polarization during the long-term cycling experiments. Fig. 6c and d shows the gas evolution and impedance of the cells after the long-term cycling. The cell with 2% PBF cell had the least gas evolved and the smallest

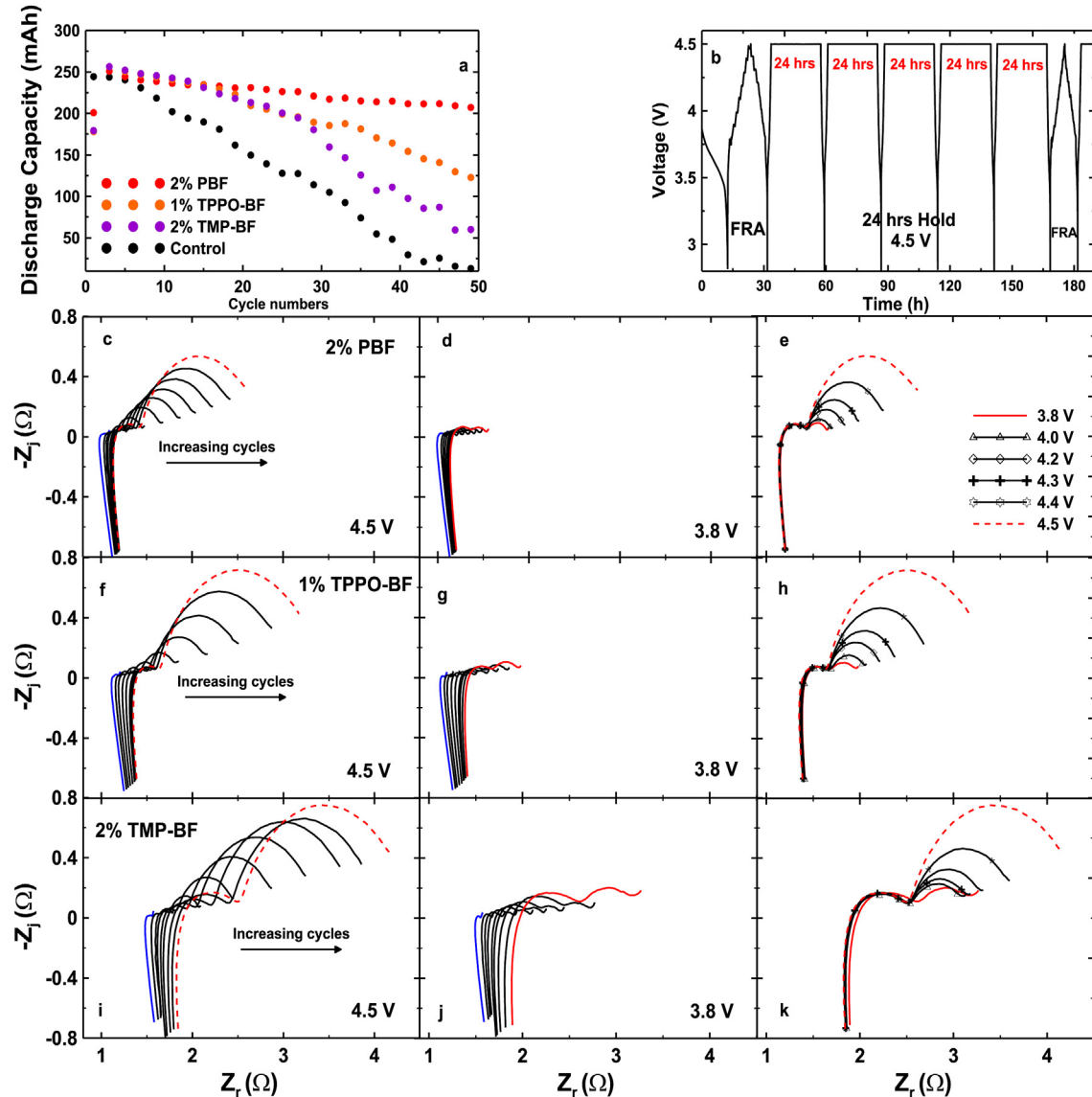


Fig. 3. (a) Discharge capacity versus cycle number for NMC442/graphite cells cycled with charge-hold-discharge protocol (C/2.5 cycling with a 24 h TOC hold at 4.5 V every cycle) at 40 °C; (b) Schematic of the testing method used for the cycle-/hold-discharge FRA protocol. (c), (d) and (e) Impedance spectra for 2% PBF cell taken at 4.5 V with cycle number increasing from red to blue and Nyquist spectra of the same cell measured at various voltage at the last cycle. (f), (g) and (h) Impedance spectra for 1% TPPO-BF cell taken at 4.5 V with cycle number increasing from red to blue and Nyquist spectra of the same cell measured at various voltage at the last cycle. (i), (j) and (k) Impedance spectra for 2% TMP-BF cell taken at 4.5 V with cycle number increasing from red to blue and Nyquist spectra of the same cell measured at various voltages at the last cycle. (For interpretation of the references to colour in this figure legend, the reader is referred to the web version of this article.)

impedance after long-term cycling.

Given that the performance of PBF-containing cells is greater than those prepared with control electrolyte or the other two acid-base adducts, it is important to investigate whether there are any differences in the chemical composition of the electrode surfaces in these cells. Fig. S3 shows that after the cycle-hold-discharge process, cells with control electrolyte, 2% TMP-BF or 1% TPPO-BF had similar XPS spectra of both lithiated graphite and NMC442 surfaces suggesting similar SEI films. Based on previous analyses, the composition of the SEIs includes lithium alkyl carbonate, lithium carbonate (Li_2CO_3), and lithium fluoride (LiF) components [24,26,39–43]. By contrast, the XPS spectra for electrodes taken from cells with 2% PBF were completely different. Significantly, the amount of LiF on the graphite surface is comparable for the control cells and those prepared with TMP-BF or TPPO-BF. This is clearly at odds with the earlier hypothesis that BF_3 adduct additives decrease

cell impedance by reacting with LiF to form the soluble electrolyte salt LiBF_4 . In contrast, the addition of PBF significantly decreases the relative amount of LiF at the graphite surface. It is possible that the addition of these BF_3 adducts in solution is insufficient to prevent the accumulation of LiF at the negative electrode surface. However, it has been suggested previously that during the SEI formation of PBF-containing cells, a reduced PBF dimer species is deposited onto the graphite surface [9]. It is therefore proposed that it is this SEI component that prevents the accumulation of LiF and, thus, limits the impedance growth on the negative electrode.

Fig. 7 shows the C 1s (a), O 1s (b), F 1s (c), 74 – 41 eV range (d) and N 1s (e) XPS core spectra of the lithiated graphite electrodes as well as the O 1s XPS core spectra of the NMC442 electrodes (f) taken from NMC442/graphite pouch cells with control and 2% PBF electrolytes at 3.5 V during formation and at 3.8 V after the cycling-hold process (Fig. 4) compared to the fresh electrode (i.e. without

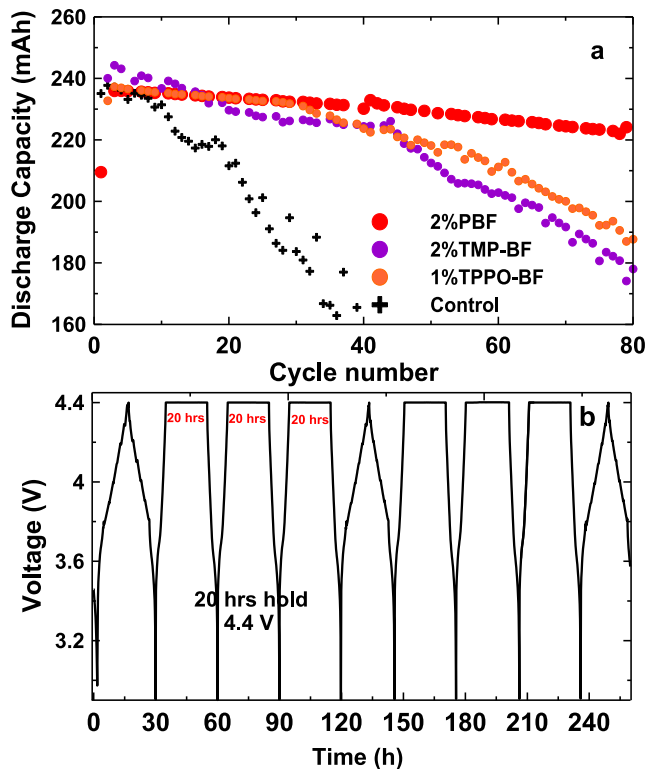


Fig. 4. (a) Discharge capacity versus cycle number for NMC442/graphite cells cycled with charge-hold-discharge protocol (C/5 cycling with a 20 h TOC hold at 4.4 V, every 3 cycles with a FRA measurement and (b) Schematic of the testing method used for the 4.4 V cycle-hold-discharge protocol.

electrolyte). In Fig. 7, the core level spectra for a given element were normalized to show the relative intensities/amount of the given element between samples. The core component assignment is described in Fig. 7 and details of the assignment can be found in previous work [24].

Fig. 7a shows that during formation at 3.5 V, the use of 2% PBF led to a significantly different C 1s spectrum compared to control electrolyte. The intensity of the graphite peak significantly decreased for control electrolyte indicating the formation of a SEI film at the graphite surface. When 2% PBF was used, however, no graphite peak was visible indicating that PBF creates a relatively thick SEI at the graphite surface compared to control electrolyte which can explain the significantly higher impedance measured after formation with 2% PBF (Fig. 1d). Also, almost no CO_3^- and CO_2^- -components were observed for 2% PBF electrolyte compared to control cells. More importantly, for 2% PBF electrolyte, the second main C 1s peak (blue, Fig. 7a) was slightly shifted to lower binding energy compared to control cell more likely due the additional contribution of C–N bonds from the PBF reduction product(s) which are formed in a 2 electron reaction [4,30] during the plateau at 2.3 V shown in Fig. 1a. The presence of nitrogen in the SEI film for 2% PBF electrolyte was confirmed by the appearance of two N 1s components that can be both attributed to C–N bonds (Fig. 7e). Although a possible pathway for the reduction of PBF in a cell to form a lithium bipyridine: BF_4^- adduct salt was previously suggested, the presence of two N 1s peaks rather than one remains unclear [9]. It is possible that multiple reduction products exist, although the three proposed in the published reaction scheme (2,2', 2,4', and 4,4' bipyridine isomers) are expected to have very similar N 1s BEs owing to the oxidation states of the nitrogen atoms in these compounds. Alternatively, it is possible that the reduced species can react further, such as through loss of a BF_3 moiety to

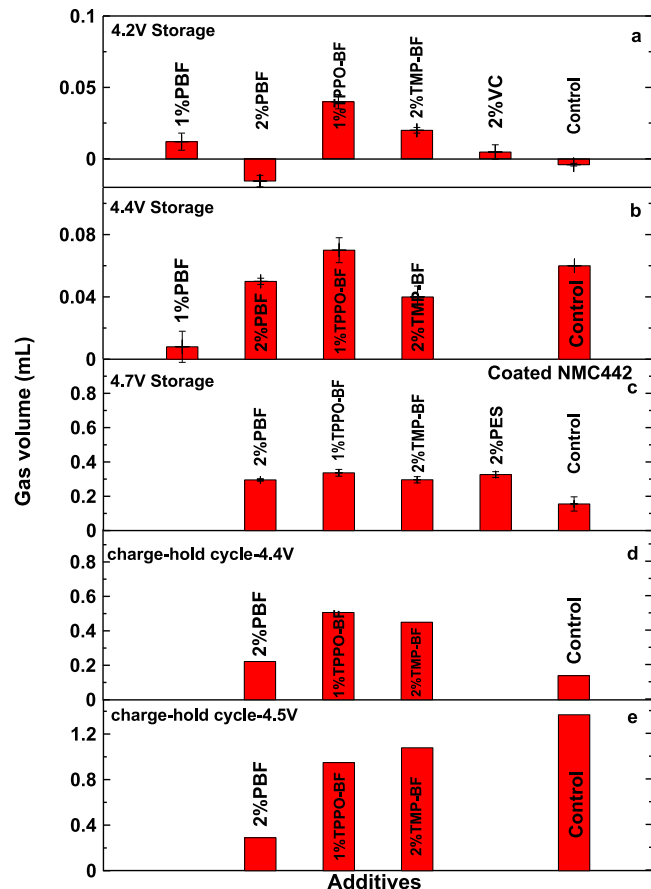


Fig. 5. Summary of volume expansion of pouch cells after storage and after charge-hold-discharge cycling presented in Fig. 2–4, respectively; (a) NMC111/graphite cells after 4.2 V storage; (b) NMC442/graphite cells after 4.4 V storage; (c) LaPO₄-coated NMC442/graphite cells after 4.7 V storage; (d) NMC442/graphite cells after 4.4 V charge-hold-discharge cycling and (e) NMC442/graphite cells after 4.5 V charge-hold-discharge cycling.

form a lithium bipyridine salt. After charge-hold-discharge cycling, the N 1s signal decreased substantially due to the covering of the PBF-derivative species by other species. Note that no boron 1s component could be definitively identified due to the overlap with the P 2s components.

Fig. 7b shows that during formation at 3.5 V, the two O 1s peaks from the CMC binder of the fresh graphite electrode were replaced by two main components. For 2% PBF electrolyte, however, the overall oxygen content was significantly reduced and the second peak was slightly shifted to lower binding energy compared to control electrolyte. The use of 2% PBF also almost suppressed the formation of ROLi and Li_2O compared to control electrolyte. These results are then in agreement with the formation of an SEI layer with a specific reactivity at graphite surface during formation. Fig. 7a and b also show that after charge-hold-discharge cycling, the use of 2% PBF electrolyte led to a more organic SEI layer with higher carbon and oxygen contents than control cells due to a much lower fluorine content from LiF (Fig. 7c). Indeed, Fig. 7c shows that the use of 2% PBF significantly decreased the production of LiF from the LiPF_6 salt during the cycling-hold process. The lower intensity of the Li 1s feature for 2% PBF electrolyte (Fig. 7d) is also in good agreement with the lower production of LiF during charge-hold-discharge cycling. Fig. 7d shows, however, the presence of an additional component for 2% PBF electrolyte at about 70 eV attributed to Ni 3p possibly due to nickel dissolution from the NMC442 electrode during the charge-hold-discharge cycling

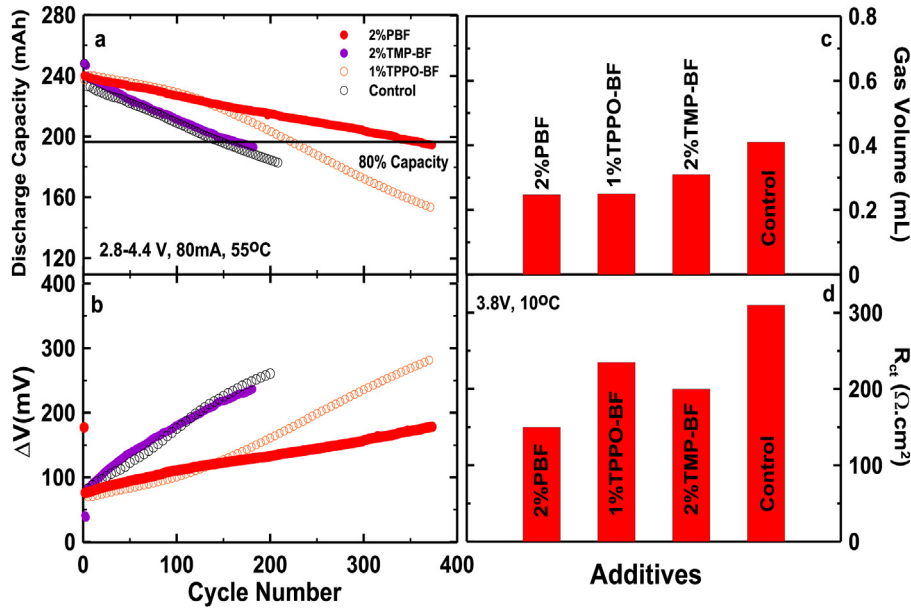


Fig. 6. (a) Discharge capacity versus cycle number for NMC442/graphite pouch cells cycled without clamps at C/3 (0.08 A) at $55. \pm 0.1$ °C between 2.8 and 4.4 V with different additives and with control electrolyte; (b) difference between average charge and discharge voltage (ΔV) of the same cells, all plotted versus cycle number; (c) gas evolution of the same cells during 55 °C long-term cycling and (d) impedance of the same cells after cycling measured at 3.8 V and $10. \pm 0.1$ °C.

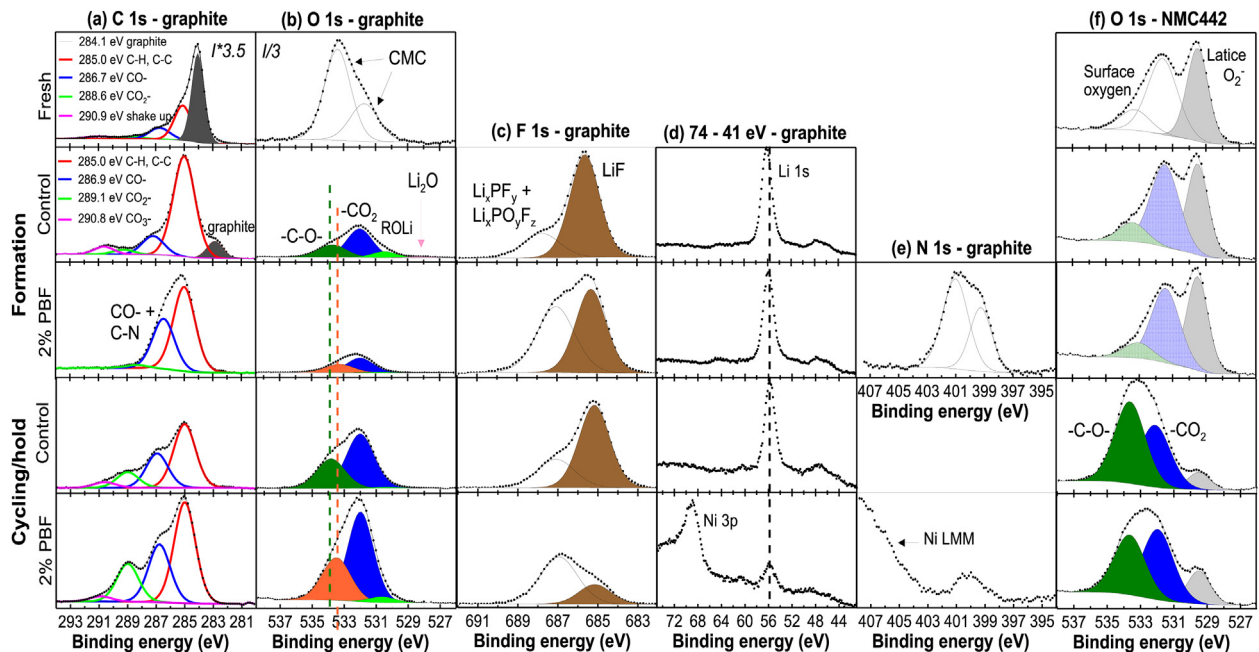


Fig. 7. Carbon 1s (a), Oxygen 1s (b), Fluorine 1s (c), 75 – 41 eV range (d), Nitrogen 1s (e) XPS core spectra of the graphite electrodes as well as Oxygen 1s XPS core spectra of the NMC442 electrodes (f), taken from NMC442/graphite pouch cells at 3.5 V during formation and at 3.8 V after the charge-hold-discharge cycling tests (Fig. 3) for cells with control and 2% PBF electrolytes.

process. The presence of Co 3p at about 60 eV and Mn 3p at about 48 eV that would be associated with the Co and Mn dissolution of the NMC442 material could not be clearly identified. This phenomenon might be due to a specific reactivity of the PBF additive during the charge-hold-discharge process compared to control electrolyte or, instead, that nickel cannot be observed for control electrolyte since less charge-hold-discharge cycles were performed (Fig. 4) before cell failure. Although this phenomenon needs further investigation, it suggests that small amounts of metal dissolution from the positive active material, here nickel, does not necessarily

mean poor cycle life as is often reported in the literature since the 2% PBF cells performed best in Fig. 3.

Fig. 7f shows that after formation at 3.5 V, no significant difference was observed in the O 1s XPS core spectra of the NMC442 electrodes for both control and 2% PBF electrolytes compared to the fresh NMC442 electrode which indicates that almost no SEI was formed at the NMC surface at this potential. This is supported by the absence of nitrogen from PBF at the NMC442 surface during formation while after the charge-hold-discharge process; two N 1s components were observed. It is hypothesized that the PBF is

reduced at the graphite surface during formation and subsequently crosses over to the NMC442 surface. After the charge-hold-discharge process, both control and 2% PBF electrolytes showed a significant decrease in the NMC feature at 529.5 eV and the two surface oxygen peaks from the fresh electrode were replaced by two new components in agreement with the formation of a SEI film at the NMC442 surface. Interestingly, when 2% PBF was used, the intensity of the NMC peak at 529.5 eV was significantly higher compared to control electrolyte suggesting a much thinner SEI film at the NMC442 surface with 2% PBF even though more charge-hold-discharge cycles were performed (Fig. 3). This result can therefore explain the lower impedance measured at the end of the charge-hold-discharge process compared to control cells (Fig. 3). This result also suggests that PBF hinders parasitic reactions at the NMC442 surface at 4.4 V which is consistent with the improved storage behavior shown in Fig. 2c.

These results indicate that the simple addition of any Lewis acid BF_3 adduct to the electrolyte solution is insufficient to improve lithium-ion battery performance. Nor is the use of a labile adduct, given that the less effective additives (TMP-BF and TPPO-BF) are more labile than PBF (Table 1). Rather, the significant difference is the use of pyridine, an aromatic amine, as the Lewis base. The tendency of PBF to reduce during SEI formation and to form a surface species, such as the bipyridine species proposed in Ref [9], is a significant difference from the other two adducts in this work, prepared from phosphine and phosphate Lewis bases. It is here proposed that it is the specific reactivity of this reduced, PBF-derived SEI component that leads to the excellent performance of cells containing PBF.

5. Conclusions

Some Lewis acid-base adducts including TMP-BF and TPPO-BF (B–O bond, low affinity constant) were synthesized using a similar method as PBF (B–N bond, high affinity constant) and studied as electrolyte additives in NMC111 or (coated and uncoated) NMC442/graphite Li-ion cells. The results indicated that PBF improves cell performance: less voltage drop during storage at 4.2 or 4.4 V; slower impedance growth during charge-hold-discharge cycling and better capacity retention during two distinct cycling protocols. The additives TMP-BF and TPPO-BF are certainly inferior to PBF, despite having the same Lewis acid (BF_3) and greater lability. XPS and electrochemical results supported the previously proposed pathway for the reduction of PBF at the graphite electrode surface during the initial charging step. Whereas the initial deposition of this PBF-derived compound leads to an initial increase in cell impedance during formation, it is here suggested that it subsequently leads to improved cell performance. The specific reactivity of this SEI component limits the formation of detrimental LiF , LiOR , and Li_2O species, decreasing impedance growth after the charge-hold-discharge cycling process. XPS also showed that the use of 2% PBF apparently hinders the degradation of both LiPF_6 and solvent during formation and in the charge-hold-discharge process in good agreement with the cycling results (Figs. 3–5). In summary, PBF including comprehensive functions from both pyridine and BF_3 outperformed TMP-BF and TPPO-BF additives in EC: EMC based electrolyte systems.

Acknowledgements

The authors acknowledge the financial support of NSERC and 3M Canada under the auspices of the Industrial Research Chairs program and the funding of NSERC under the Automotive Partnership Canada program. The authors thank Dr. Jing Li of BASF for

providing some of the solvents and salts used in this work.

Appendix A. Supplementary data

Supplementary data related to this article can be found at <http://dx.doi.org/10.1016/j.jpowsour.2016.08.048>.

References

- [1] M. Broussely, Ph. Biensan, F. Bonhomme, Ph. Blanchard, S. Herreyre, K. Nechev, R.J. Staniewicz, *J. Power Sources* 146 (2005) 90.
- [2] Y.M. Lee, Y.-G. Lee, Y.-M. Kang, K.Y. Cho, *Electrochim. Solid-State Lett.* 13 (2010) A55–AA58.
- [3] J.C. Burns, N.N. Sinha, Gaurav Jain, Hui Ye, Collette M. VanElzen, W.M. Lamanna, A. Xiao, Erik Scott, J. Choi, J.R. Dahn, *J. Electrochem. Soc.* 159 (2012) A1095–A1104.
- [4] M. Nie, J. Xia, J.R. Dahn, *J. Electrochim. Soc.* 162 (2015) A1186–A1195.
- [5] M. Nie, J. Xia, J.R. Dahn, *J. Electrochim. Soc.* 162 (2015) A1693–A1701.
- [6] M. Nie, J. Xia, J.R. Dahn, *J. Electrochim. Soc.* 162 (2015) A2066–A2074.
- [7] L. Ma, J. Self, M. Nie, S. Glazier, D.Y. Wang, Y.S. Lin, J.R. Dahn, *J. Power Sources* 299 (2015) 130–138.
- [8] L.D. Ellis, J. Xia, A.J. Louli, J.R. Dahn, *J. Electrochim. Soc.* 163 (2016) A1686–A1692.
- [9] D.S. Hall, M. Nie, L.D. Ellis, S.L. Glazier, S. Hyatt, R. Petibon, A. Xiao, W.M. Lamanna, K. Smith, I.G. Hill, J.R. Dahn, *J. Electrochim. Soc.* 163 (2016) A773–A780.
- [10] X. Zuo, C. Fan, J. Liu, X. Xiao, J. Wu, J. Nan, *J. Electrochim. Soc.* 160 (2013) A1199–A1204.
- [11] S.S. Zhang, *J. Power Sources* 162 (2006) 1379–1394.
- [12] M. Lashkari, M.R. Arshadi, *Chem. Phys.* 299 (2004) 131–137.
- [13] M.A. Veloz, I.G. Martinz, *Corrosion* 62 (2006) 283–292.
- [14] C. Laurence, J.-F. Gal, *Lewis Basicity and Affinity Scales*, John Wiley & Sons, Ltd, 2009.
- [15] P.A. van der Meulen, H.A. Heller, *J. Am. Chem. Soc.* 54 (1932) 4404–4406.
- [16] Y. Wang, M. Zhang, U. V. Sacken, B. M. Way, (2000) US Patent 6,045,948.
- [17] M. Matsui, (2014) US patent 8,765,294.
- [18] K.J. Nelson, G.L. d'Eon, A.T.B. Wright, L. Ma, J. Xia, J.R. Dahn, *J. Electrochim. Soc.* 162 (2015) A1046–A1054.
- [19] J. Xia, Z. Lu, J. Camardese, J.R. Dahn, *J. Power Sources* 306 (2016) 516–525.
- [20] K.J. Nelson, D.W. Abarbanel, J. Xia, Z. Lu, J.R. Dahn, *J. Electrochim. Soc.* 163 (2016) A272–A280.
- [21] J. Li, R. Petibon, S. Glazier, N. Sharma, W. Pang, V.K. Peterson, J.R. Dahn, *Electrochim. Acta* 180 (2015) 234–240.
- [22] N.N. Sinha, T.H. Marks, H.M. Dahn, A.J. Smith, J.C. Burns, D.J. Coyle, J.J. Dahn, J.R. Dahn, *J. Electrochim. Soc.* 159 (2012) A1672–A1681.
- [23] C.P. Aiken, J. Xia, D.Y. Wang, D.A. Stevens, S. Trussler, J.R. Dahn, *J. Electrochim. Soc.* 161 (2014) A1548–A1554.
- [24] L. Madec, J. Xia, R. Petibon, K.J. Nelson, J.-P. Sun, I.G. Hill, J.R. Dahn, *J. Phys. Chem. C* 118 (2014) 29608–29622.
- [25] D.A. Shirley, *Phys. Rev. B* 5 (1972) 4709–4714.
- [26] M. Nie, D. Chalasani, D.P. Abraham, Y. Chen, A. Bose, B.L. Lucht, *J. Phys. Chem. C* 117 (2013) 1257–1267.
- [27] J. Self, C.P. Aiken, R. Petibon, J.R. Dahn, *J. Electrochim. Soc.* 162 (2015) A796–A802.
- [28] K. Xu, *Chem. Rev.* 104 (2004) 4303–4418.
- [29] D. Aurbach, K. Gamolsky, B. Markovsky, Y. Gofer, M. Schmidt, U. Heider, *Electrochim. Acta* 47 (2002) 1423–1439.
- [30] O. Matsuoka, A. Hiwara, T. Omi, M. Toriida, T. Hayashi, C. Tanaka, Y. Saito, T. Ishida, H. Tan, S.S. Ono, S. Yamamoto, *J. Power Sources* 108 (2002) 128–138.
- [31] J. Self, D.S. Hall, L. Madec, J.R. Dahn, *J. Power Sources* 298 (2015) 369–378.
- [32] L. Madec, R. Petibon, J. Xia, J.-P. Sun, I.G. Hill, J.R. Dahn, *J. Electrochim. Soc.* 162 (2015) A2635–A2645.
- [33] L. Ma, J. Xia, J.R. Dahn, *J. Electrochim. Soc.* 161 (2014) A2250–A2254.
- [34] C.H. Chen, J. Liu, K. Amine, *J. Power Sources* 96 (2001) 321.
- [35] J. Syzdek, M. Marcinek, R. Kostecki, *J. Power Sources* 245 (2014) 739–744.
- [36] R. Younesi, A.S. Christiansen, R. Scipioni, D.-T. Ngo, S.B. Simonsen, K. Edström, J. Hjelm, P. Norby, *J. Electrochim. Soc.* 162 (2015) A1289–A1296.
- [37] M. Metzger, C. Marino, J. Sicklinger, D. Haering, H.A. Gasteiger, *J. Electrochim. Soc.* 162 (2015) A1123–A1134.
- [38] R. Petibon, L. Madec, D. W. Abarbanel, J. R. Dahn, submitted to *J. Power Sources*.
- [39] L. Bodenes, R. Dedryvère, H. Martinez, F. Fischer, C. Tessier, J.-P. Péres, *J. Electrochim. Soc.* 159 (2012) A1739–A1746.
- [40] L. El Ouatani, R. Dedryvère, C. Siret, P. Biensan, S. Reynaud, P. Iratçabal, D. Gonbeau, *J. Electrochim. Soc.* 156 (2009) A103–A113.
- [41] L. El Ouatani, R. Dedryvère, C. Siret, P. Biensan, D. Gonbeau, *J. Electrochim. Soc.* 156 (2009) A468–A477.
- [42] L. El Ouatani, R. Dedryvère, J.-B. Ledeuil, C. Siret, P. Biensan, J. Desbrères, D. Gonbeau, *J. Power Sources* 189 (2009) 72–80.
- [43] J.T. Lee, N. Nitta, J. Benson, A. Magasinski, T.F. Fuller, G. Yushin, *Carbon* 52 (2013) 388–397.